Atmos. Meas. Tech. Discuss., https://doi.org/10.5194/amt-2017-413
Manuscript under review for journal Atmos. Meas. Tech.
Discussion started: 4 December 2017

Atmospheric Measurement Techniques Discussions

Cloud heterogeneity effects on cloud and aerosol above cloud properties retrieved from simulated total and polarized reflectances

Céline Cornet[1], Laurent C-Labonnote[1], Frédéric Szczap[2], Lucia Deaconu[1], Fabien Waquet[1], Frédéric Parol[1], Claudine Vanbauce[1], François Thieuleux[1], Jérôme Riédi[1]

[1]Université Lille, CNRS, UMR 8518 - LOA - Laboratoire d'Optique Atmosphérique, F-59000 Lille, France
[2]Université Clermont Auvergne, CNRS, UMR 6016, Laboratoire de Météorologie Physique, F-63000 Clermont-Ferrand, France

Correspondence to: Céline Cornet (celine.cornet@univ-lille1.fr)

Abstract. Simulations of total and polarized cloud reflectance angular signatures such as the ones measured by the multi-angular and polarized radiometer POLDER3/PARASOL are used to evaluate cloud heterogeneity effects on cloud parameter retrievals. Effects on optical thickness, cloud albedo, effective radius and variance of the cloud droplet size distribution and aerosol above cloud optical thickness are analyzed. Three different clouds having the same mean optical thicknesses were generated: the first one with a flat top, the second one with a bumpy top and the last one with a fractional cloud cover. At small scale (50 m), for oblique solar incidence, the illumination effects lead to higher total but also polarized reflectances. The polarized reflectances even reach values that cannot be predicted by the 1D homogeneous cloud assumption. At the POLDER scale (7 km x 7 km), the angular signature is modified by a combination of the plane-parallel bias and the shadowing and illumination effects. In order to quantify effects of cloud heterogeneity on operational products, we ran the POLDER operational algorithms on the simulated reflectances to retrieve the cloud optical thickness and albedo. Results show that the cloud optical thickness is greatly affected: biases can reach up to -70%, -50% or +40% for backward, nadir and forward viewing directions respectively. Concerning the cloud albedo, the errors are smaller, between -4.7% for solar incidence angle of 20° and up to about 8% for solar incidence angle of 60°. We also tested the heterogeneity effects on new algorithms that allow retrieving cloud droplet size distribution and cloud top pressures and also aerosol above clouds. Contrarily to the bi-spectral method, the retrieved cloud droplet size parameters are not significantly affected by the cloud heterogeneity, which proves to be a great advantage of using polarized measurements. However the cloud top pressure obtained from molecular scattering in the forward direction can be biased up to 120 hPa (around 1 km). Concerning the aerosol optical thickness (AOT) above cloud, the results are different depending on the available angular information. Above the fractional cloud, when only side scattering angles are available, the AOT can be underestimated because of the plane-parallel bias. For solar zenith angle of 60°, on contrary, it is overestimated because the polarized reflectances are increased in forward directions.

Atmos. Meas. Tech. Discuss., https://doi.org/10.5194/amt-2017-413
Manuscript under review for journal Atmos. Meas. Tech.
Discussion started: 4 December 2017

Atmospheric Measurement Techniques Discussions

1 Introduction

Cloud properties such as effective radius, optical thickness and cloud albedo are key parameters for studies concerning cloud radiative effects and hydrological cycle of Earth climatic system. In the context of climate change, these properties may be modified and result in a feedback, the sign of which remains largely uncertain. In parallel, anthropogenic activities modify the aerosol loading in the atmosphere and consequently play an important role on cloud through the indirect radiative effects of aerosols (Twomey et al. 1977). To better detect and understand cloud evolutions, it is essential to monitor their properties from global observation.

Currently, several satellite radiometers use solar and infrared reflectances to infer cloud parameters. Generally, cloud optical thickness (COT) and cloud albedo are obtained from visible channels. Depending on instrument capabilities, the effective radius can be retrieved jointly with the optical thickness from a combination of visible and near-infrared measurements (Nakajima and King, 1990) as it is done in the operational algorithm of the Moderate Resolution Imaging Radiometer (MODIS Platnick et al., 2003). These parameters can also be retrieved separately from multi-viewing total and polarized measurements (Buriez et al., 1997; Bréon and Goloub, 1998) as implemented or under implementation for the Polarization and Directionality of the Earth's Reflectances Radiometer, (POLDER, Deschamps et al., 1994).

For computation time and simplicity reasons, all these operational algorithms assume that clouds are flat, homogeneous and horizontally infinite, which is quite far from the reality. Numerous studies presented for example in Davis and Marshak (2010) or in Marshak and Davis (2005) showed that this assumption can lead to large errors on the retrieved cloud parameters. For example, the cloud optical thickness can be affected by the so-called plane-parallel bias induced by the sub-pixel heterogeneity and the non-linear relationship between reflectances and optical thickness. This bias usually leads to an effective optical thickness lower than the mean optical thickness (Cahalan, 1994; Szczap et al., 2000a). The sub-pixel optical thickness heterogeneity can also cause a positive bias on the mean effective radius retrieved following the bi-spectral technique (Szczap et al., 2000b; Zhang et al., 2012), whereas the sub-pixel microphysical heterogeneity, not studied in this paper, leads on the contrary to an underestimation of the effective radius (Marshak et al., 2006). The bias on effective radius can thus be positive or negative depending on sub-pixel heterogeneity of the cloud optical thickness and effective radius (Zhang et al., 2016).

In addition to the sub-pixel heterogeneity, Loeb and Davies (1996) detected an increase of the retrieved optical thickness from AVHRR correlated with the solar zenith angle elevation. Indeed, for oblique solar illumination, more energy is transmitting through the clouds along the cloud side (or bump), and leads to an increase of the upward reflectances and consequently to higher cloud optical thicknesses retrieved under the homogeneous cloud assumption. This effect is combined with angular effects, known as 3D effects, which depends on the sensor viewing direction. Again, in the backward scattering direction, parts of the cloud sides are illuminated by the sun and lead to a larger retrieved optical thickness value. Inversely, in viewing directions close to the forward scattering directions, some parts of the cloud are in the shadow resulting in smaller optical thickness or larger effective radius. This angular signature was observed on the retrieved cloud optical thickness by

several radiometers such as AVHRR (Loeb and Coakley, 1998), MODIS (Varnai and Marshak, 2002) and POLDER (Buriez et al., 2001; Zeng et al., 2012).

Therefore, depending on the cloud heterogeneity, solar zenith angle and viewing geometry, cloud parameters (i.e. optical thickness and effective radius) can be either under- or overestimated. Several studies based on simulations of total reflectances were made at the scale of 1 km corresponding to a moderate resolution radiometer such as MODIS or the GLobal Imager (GLI/ADEOS2) to assess errors for liquid water clouds on optical thickness (Iwabuchi and Hayasaka, 2002; Zinner and Mayer, 2006) or on effective radius (Zhang et al., 2012). Kato et al. (2006) analyzed in addition the error on the cloud albedo, which is an important parameter for cloud radiative budget studies. At 1 km pixel size, they found significant errors ranging between -0.3% to 14% (-5% to 30%) from nadir (oblique view) depending on the cloud heterogeneity. Some recent studies were also made in case of ice clouds and found non negligible errors on retrieved COT from IR measurements (Fauchez et al., 2015) or from visible and near-infrared measurements (Zhou et al., 2017)

In this paper, we investigate the impact of cloud heterogeneities on retrieved parameters on observations from the POLarization and Directionality of Earth Reflectance radiometer, POLDER, which was on board the platforms ADEOS1 in 1999, ADEOS2 in 2002 and PARASOL between 2005 and 2013. POLDER/PARASOL allows to measure multi-angular total reflectances from 443 to 1020 nm and multi-angular polarized reflectances for three channels (490, 670 and 865 nm).

A review of the POLDER capabilities for cloud measurements and retrieval are presented in (Parol et al., 2004). Comparisons with MODIS cloud products were analyzed for cloud fraction in Zeng et al. (2011), for cloud phase in Zeng et al. (2013) and cloud optical thickness in Zeng et al. (2012). In the latter, the plane-parallel bias and 3D cloud effects were observed in the COT values retrieved from multi-angle measurements under oblique solar illumination, lower COT were retrieved in the forward viewing direction and larger COT in the backward viewing direction (Figure 8 and 9 in Zeng et al. (2012)). Reflectances simulations from known cloud properties help to understand quantitatively the errors or biases on the retrieved cloud properties. In addition, assessment of POLDER algorithms will be helpful in a near future as the Multi-viewing, Multi-Channel, Multi-Polarization Imaging mission (3MI), a POLDER type follow-on instrument is planned to be part of the future generation of EUMETSAT polar satellites, EPS-SG (Marbach et al., 2015).

Accordingly, total but also polarized reflectances were simulated at a small scale (50 m) from synthetic 3D cloud fields and averaged at the POLDER pixel size (7 km x 7 km) to simulate POLDER measurements. The different clouds used in our study and presented in section 2 are generated using an enhanced version of the 3DCLOUD model (Szczap et al., 2014; Alkassem et al., 2017). The POLDER cloud operational algorithm described in (Buriez et al., 1997) is then used to retrieve the COT and the cloud albedo. Results are presented in section 3.

Contrarily to MODIS, POLDER does not make measurements in the near infrared to get information on cloud particle size. The two first moments of the cloud droplet distribution are obtained from polarized angular measurements (Bréon and Goloub, 1998; Breon and Doutriaux-Boucher, 2005) as well as the cloud top pressure (Goloub et al., 1994). Polarized reflectances measurements are also used for cloud droplets retrievals by the Research Scanning Polarimeter (Alexandrov et

al., 2012). Cloud heterogeneity effects on polarized measurements of liquid clouds have been studied for a single flat cloud in (Cornet et al., 2013) and almost no effects were found. Here, we go further and present in section 4 differences between 3D and 1D polarized angular reflectances for different clouds and geometries. Consequences of 3D cloud radiative effects on the effective radius, effective variance cloud top pressure retrieval are presented in section 5. The POLDER polarized reflectances are also used to retrieve the aerosols above cloud properties (Waquet et al., 2013). The cloud heterogeneity effects on aerosol above cloud retrieval are also studied and presented in section 5. Conclusions are summarized in section 6.

2 Description of the synthetic generated clouds and radiative transfer simulations

The clouds used in this study have been generated with the 3DCLOUD model (Szczap et al., 2014; Alkassem et al., 2017). 3DCLOUD is a fast and flexible algorithm designed for generating realistic 3D extinction or 3D optical depth for stratocumulus, cumulus and cirrus cloud fields. 3DCLOUD cloud fields share some pertinent statistical properties observed in real clouds such as a gamma distributed optical depth and the Fourier spectral slope β close to −5/3 between the smallest scale of the simulation to the outer scale L_{out} where the spectrum becomes flat. In addition, the user can specify the mean optical depth COT, the inhomogeneity parameter ρ (standard deviation of COT normalized by the mean of COT) and the cloud coverage C. In a first step, 3DCLOUD solves drastically simplified basic atmospheric equations and integrates user's prescribed large-scale meteorological profiles (humidity, pressure, temperature and wind speed), in order to simulate 3D cloud structures of liquid water content (LWC). In a second step, the amplitude of the wavelet coefficient of the extinctions are manipulated with a 3D Wavelet transform of the whole 3D cloudy volume to constrain the intensity of the mean COT, ρ, β and L_{out} (Alkassem et al., 2017).

Here, we generated three clouds fields composed of 140 x 140 pixels with an initial horizontal resolution of 50 m resulting to a 7 km x 7 km field, which corresponds to a POLDER pixel size. The three generated clouds have the same mean optical thickness close to 10 at 865 nm. The flat and bumpy clouds have the same heterogeneity parameter computed from 50 m-pixel (optical standard deviation over the mean optical thickness) of 0.6 and the fractional cloud cover is set to 1. The fractional cloud has a fractional cloud cover fixed to 0.76 and a heterogeneity parameter equal to 1.12 if the heterogeneity parameter (optical standard deviation over the mean optical thickness) is computing including the zeros or 0.95 if it is computing only with the cloudy pixels (Szczap et al., 2014). Figure 1 shows the horizontal cloud optical thickness field and a vertical profile through each cloud. In this study, we focus on the effects of the optical thickness heterogeneity, which is supposed, in real cloud, to be more important than the microphysical heterogeneity. Consequently, the cloud size distribution is assumed uniform everywhere in the cloud and follows a log-normal distribution with an effective radius of 11 μm and an effective variance of 0.02.

From these 3D cloud fields, we simulated total and polarized reflectances R for viewing zenith angle θ and viewing azimuthal angle φ defined as :

Atmos. Meas. Tech. Discuss., https://doi.org/10.5194/amt-2017-413
Manuscript under review for journal Atmos. Meas. Tech.
Discussion started: 4 December 2017

Atmospheric Measurement Techniques Discussions

$$R(\theta,\varphi) = \frac{\pi I(\theta,\varphi)}{F_0 \cos\theta_0},$$

where $I(\theta,\varphi)$ are the radiance in W.m^{-2}.Sr^{-1}, F_0 the solar flux in W.m^{-2} and θ_0 the zenith solar incidence angle.

Reflectances for three solar incidence angles 20°, 40° and 60° are computed with the 3D radiative transfer model 3DMCPOL (Cornet et al., 2010). At this stage, molecular scattering is integrated but no aerosols. To remain consistent with assumptions made within POLDER operational algorithm, an oceanic surface with a wind speed of 7 m.s-1 is included for total reflectances while a black surface is included for polarized reflectances. As POLDER measures up to 16 directions, we simulate reflectances for 16 POLDER typical zenith observation angles in the solar plane. Total reflectances of the three clouds are presented in Figure 3 (first column) with a 50 m spatial resolution for a solar incidence angle of 60° in the cloudbow direction (40° from the backward direction). Polarized reflectances fields are discussed in section 4.1.

3 Impacts on total reflectances and consequences for optical thickness and cloud albedo retrieval

We averaged spatially the 50 m resolution reflectances fields at 7 km x 7 km to mimic the radiometer measurements and applied the POLDER operational algorithm on these synthetic measurements to obtain cloud optical thickness and albedo. In order to assess the retrieval errors due to the cloud homogeneous assumption without biases due to differences in reflectance computations, we also computed the 1D reflectances of the equivalent homogenous cloud. The mean optical thickness, and the cloud top and base altitudes corresponding to the maximal and minimal altitudes of the heterogeneous clouds are used.

Figure 2 summarizes the results obtained for the retrieved cloud optical thickness for the three solar zenith angles and the four cases, e.g. the homogeneous (1D), the flat, the bumpy and the fractional cloud. Note that in the three cases, the operational algorithm retrieves a cloud cover equal to one. The optical thicknesses are plotted as a function of sensor zenith angle with negative value corresponding to backward scattering directions and positive value to forward scattering directions. The homogeneous cloud values (1D) are only plotted for control and we observe logically that the retrieved value is almost constant and close to 10, independently of the solar incidence angle, since the same assumption (eg 1D homogeneous cloud) is used in both the direct simulation and retrieval algorithm. Slight differences appear because of inclusion of aerosol optical thickness in the forward model used to build the look-up table (Buriez et al., 1997) but not into our simulations. The small angular difference in the backward direction at 20° can be attributed to interpolation in the LUT.

Looking at results concerning the heterogeneous clouds (3D), we clearly note, in the angular range between about -30° and +30°, the well-known plane-parallel bias, which leads to retrieve optical thicknesses lower than the mean optical thickness. At nadir view, the relative error is between -10 and -20% both for the flat and bumpy cloud and is much larger for the fractional cloud, between -35 and -50%. The flat and bumpy clouds were built with the same heterogeneity parameter (ρ=0.6) whereas the fractional cloud has a larger heterogeneity parameter including the zeros (ρ=1.12) due to its fractional

nature. That confirms that heterogeneity parameters can be at first order used to characterize plan-parallel bias (Cahalan et al. 1994, Szczap et al., 2000a).

For solar zenith angle (SZA) equal to 20°, the retrieved optical thickness is almost independent of the observation geometry whatever the cloud type, while for SZA=60°, differences are important according to the viewing direction. We note indeed a strong decrease of the retrieved optical thickness value in the forward scattering direction leading to a relative bias on the retrieved optical thickness between -40% for the flat and bumpy cloud and -70% for the fractional cloud. On the contrary, we can notice an increase of the retrieved optical thickness value in the backscatter direction (relative bias ranging from +3% for the flat cloud, +43% for the bumpy cloud and +21% for the fractional cloud). This angular behavior was already simulated by several authors at the resolution of 1 km (Loeb et al., 1998; Varnai, 2000; Iwabuchi and Hayasaka, 2002; Zinner and Mayer, 2006) and agrees pretty well with POLDER observations (Buriez et al., 2001; Zeng et al., 2012). In the backscatter directions, the cloud sides illuminated by the sun making the cloud brighter than in the forward direction where, on the contrary, cloud sides are in the shadow (Varnai and Davies, 1999). These effects are visible for the bumpy cloud but are much less pronounced for the flat cloud. The heterogeneity parameter seems thus well adapted to characterize quantitatively the plane-parallel bias (Szczap et al., 2000a) but not sufficient to characterize the amplitude of the 3D effects. Indeed, the flat and bumpy clouds, which are characterized by the same heterogeneity parameter value show close plane-parallel bias (about -10-20% for nadir view) but quite different amplitudes of the 3D effects, especially in the backward direction for SZA=60°. We note also that this error in the backward direction is larger for the bumpy cloud (about +40%) compared to the fractional cloud (about +20%) because for the latter the plane-parallel bias is stronger (about -40% at nadir view).

The following step in the POLDER operational algorithm consists in computing the cloud albedo, corresponding to the upward flux normalized by the solar incident flux, from the retrieved cloud optical thickness using look-up tables (Buriez et al., 1997). The cloud albedo is not derived from a single view as computed in Kato et al. (2006) at 1 km x 1 km but from every viewing angles. The multi-angular capabilities of POLDER allow then averaging of the different values using a directional weighting function. The aim of this weighting function is to limit the influence of directions for which the microphysical or 3D effects can be important as for example in the cloudbow, glory and forward directions (Buriez et al., 2005).

Note that cloud albedos retrieved with the algorithm from 3D reflectances and from 1D reflectances are not comparable. Indeed, because of the plane-parallel bias, simulated 3D reflectances are lower than the 1D ones, the retrieved optical thickness is an effective optical thickness lower than the averaged one (Figure 2). Consequently, the albedos recomputed in the POLDER algorithm (using the 1D cloud assumption) are lower than the one obtained from the 1D reflectances. Contrarily, using 1D cloud radiative model in the inversion and in the direct computation as it is done in the operational algorithm, is coherent and leads to a sound cloud albedo. The plane-parallel bias is indeed almost cancelled.

However, some angular (3D) effects can still lead to a bias on the retrieved albedo values. In order to estimate this bias for each 3D heterogeneous cloud fields, we compare the retrieved POLDER algorithm albedos with the ones directly computed

with the 3DMCPOL radiative transfer model. Albedos are simulated simply by summing the proportion of the Monte-Carlo photons going up at the top of atmosphere.

Values of the computed and retrieved albedos and their relative differences are indicated in Table 1. The first line (homogeneous cloud) shows very good consistency between the 3DMCPOL radiative transfer code and the one used for the POLDER operational algorithm. Relative differences between computed and retrieved albedos remain smaller than 0.5%.

For SZA= 20°, the POLDER operational algorithm underestimates slightly the cloud albedo for the flat and bumpy cloud with relative differences under -2.5%. The relative is slightly larger for the fractional cloud (-4.7%). The relative differences are quite low compared to optical thickness errors because, as explained above, the same cloud model (i.e the homogeneous cloud) is used to retrieve and to compute the cloud albedo. The slight underestimation of the retrieved albedo comes from differences in the non-linear relationship (curvature degree) between reflectances and albedo in function of the optical thickness. It involves that effects of the plane-parallel bias is not the same for reflectances and albedos. Inversely, for SZA = 60°, the cloud albedo is overestimated by 2.35 % for the flat cloud case and 7.88% for the fractional cloud case because illumination effects in the backscattering direction are not completely cancelled by the weighting function.

At SZA=40°, negative differences due to the plane parallel biases are on contrary almost cancelled by illumination effects for bumpy and fractional cloud leading to very small errors of -0.26% and +0.13% respectively.

4. Differences between 3D and 1D polarized reflectances and consequences on microphysical distribution, cloud pressure and aerosol above cloud retrievals

4.1 Cloud heterogeneity effects on polarized reflectances

As previously, we simulated using 3DMCPOL, the polarized reflectances for the three wavelengths used in the POLDER retrieval algorithms (e.g. 490, 670 and 865 nm). Total and polarized reflectances at 490 nm for 50 m resolution are presented in Figure 3 (second and third columns) for SZA=60°. First of all, we can see that for flat cloud, the polarized reflectance field appears smoother than the total reflectance field. As polarized reflectances “saturate” for optical thickness greater than about 3, all cloudy pixels with higher optical thickness provide almost the same polarized reflectance. Therefore, cloud heterogeneity effects are visually less discernible on polarized reflectance fields comparing to the total reflectances fields.

For the bumpy or fractional clouds, the polarized reflectance field appears much rougher. In the cloudbow viewing directions (second column), some parts of the cloud facing to the sun appear brighter and other parts in the shadow darker. At this small spatial scale (50 m), a large part of the total amount of pixels exhibits polarized reflectance higher than the maximum value predicted by the 1D homogeneous cloud model (yellow pixels): at 490 nm, their ratio reaches 41% of the total number of pixels for the flat cloud, 52% for the bumpy cloud and 38% for the fractional cloud. This phenomenon of illumination and shadowing was already highlighted with simply a step cloud in Cornet et al. (2010).

In the forward direction (Θ=60°) at 490 nm (third column in Fig.3), the “shadows area” are not dark anymore contrarily to the total reflectances pictures (first column in Fig.3) and appear even brighter than cloudy part. For short wavelength and

Atmos. Meas. Tech. Discuss., https://doi.org/10.5194/amt-2017-413
Manuscript under review for journal Atmos. Meas. Tech.
Discussion started: 4 December 2017

forward scattering angles, molecular signal is stronger than the cloud signal and thus enhances the polarized signal in the shadow parts.

In Figure 4, we plotted the average polarized reflectances as would be measured by POLDER at 7 x 7 km, as function of the scattering angle Θ for a solar zenith angle SZA=60°, and for the three wavelengths. As we can see in Figure 4a, the main differences between homogeneous and heterogeneous cloud appear in the cloudbow direction (Θ=140°) and in the forward direction (Θ < 80°). In the cloudbow directions, the 3D polarized reflectances are lower than the 1D ones for the three clouds. As for total reflectances, this is mainly due to the plane-parallel bias. In these directions, the relative differences (Figure 4b) are about -9%, -12% and -35% for the flat, bumpy and fractional cloud respectively. We note that the relative difference is slightly lower for 490 nm because of the smoothing effects by molecular scattering above the cloud.

In the forward scattering direction, the consequences of the 3D effects in terms of absolute polarized reflectances appear differently according to the wavelength. At 490 nm, the 3D effects enhance the absolute polarization, while at 865 nm they reduce it. At 490 nm, atmospheric molecular scattering is very strong. The 3D polarized reflectances appear greater than the 1D ones because, as seen in Figure 3, the polarization in the shadow parts of the cloud is enhanced by this molecular scattering. At 865 nm, the shadow parts appear dark with small positive values that reduce the negative polarization of the cloud and consequently the absolute polarization. The relative difference (Figure 4b) are consequently positive for 490 nm (about +55% for the fractional cloud) and negative for 865 nm (about -75% for the fractional cloud). At 670 nm, the polarized reflectance in the shadow part is only slightly enhanced by the molecular scattering but sufficiently compared to 865 nm. Polarized reflectances become thus positive for the fractional cloud but not for the flat and bumpy clouds. Note that in the backward direction, the polarized reflectances are very weak so no heterogeneity or 3D effects can be detected.

Figures 3 and 4 illustrate results obtained for simulations done for SZA=60°. 3D cloud radiative effects are thus quite important, particularly in the forward direction, but it is important to note that such 3D effects are weaker for smaller SZA and almost no present for SZA=20°.

4.2 Consequences for droplet size distribution and cloud top pressure retrievals

The polarized signal is used as input of a POLDER retrieval algorithm developed to retrieve effective radius, effective variance and cloud top pressure. It uses the polarized information as presented in Bréon and Goloub (1998). The position of the cloudbow as well as the position of the surnumerary bows gives information on the effective radius. The amplitude of the surnumerary bows gives information on the effective variance of the cloud droplet size distribution. For cloud top pressure, the algorithm uses the information given by the molecular scattering which depends, in the forward scattering directions, on the atmospheric air mass factor (Goloub et al., 1994). The algorithm, under implementation in the POLDER operational algorithm, is based on an optimal estimation method (Rodgers, 2000) and provides errors associated to each of the retrieved parameters. It is also possible to add in the forward model variance-covariance matrix an error due to the non-retrieved parameter. For the misrepresentation of 3D effects, we add 7.5% error in the cloudbow direction and 5% elsewhere.

The retrieved values obtained with this algorithm based on the homogeneous cloud assumption, are presented in Table 2. As previously, we use again the homogeneous cloud (1D cloud) to check the consistency of our simulations. For all clouds, even if differences on polarized reflectances are quite large, bias on retrieved effective radius and effective variance are not significant. The algorithm is able to retrieve an effective radius of 11 μm and an effective variance of 0.02 with relative error compared to the input under 2.6 % and 2.1% respectively (see table 2). Indeed, as the cloud heterogeneity effects do not modify the cloudbow position and the number of surnumerary bows, the retrieval of the droplet size distribution parameters is not really affected by 3D effects. This is a fundamental advantage of the polarized measurements compared to the bi-spectral method (Zhang et al., 2012), usually used when visible and shortwave infrared wavelength are available. We note, however that, the cost function, which is the root mean square difference between the model and measurements weighted by the respective variance-covariance matrix is much more important for 3D clouds. For the bumpy and fractional cloud, the algorithm does even not converge meaning that the direct model is not able to represent the signal within the allocated uncertainties.

The main impact of cloud heterogeneities appears for cloud top pressure retrieval. Note that 1D values are different because the cloud top altitude (corresponding to the highest altitude of the heterogeneous cloud) is not exactly the same for the three input clouds. Comparisons were made for the equivalent homogeneous cloud by adjusting the cloud top altitude. As already explained, the polarized reflectance in the shortwave wavelengths (490 nm) is very high because of molecular scattering. The retrieval of the cloud top pressure is based on the amount of molecular scattering occurring above the cloud when looking in forward scattering (for scattering angle ranging between 60 and 120 degrees). Consequently, as shadowing effects modify the polarized reflectances in forward scattering direction, the cloud top pressure retrieval is impacted, especially for the fractional and bumpy cloud. The difference can reach +123 hPa, which means that cloud seems to be about 1 km lower.

4.3 Impacts for aerosol above cloud retrieval

Polarized reflectances of POLDER are also used to retrieve aerosol optical thickness (AOT) of an aerosol layer above cloud (Waquet et al., 2013, 2009). The detection of aerosol above cloud scenes is based on the difference between Rayleigh pressure that is enhanced by aerosol scattering, and oxygen cloud top pressure (Waquet et al., 2009). The AOT above cloud is next retrieved using the fast algorithm of (Waquet et al., 2013). Information on AOT is given by the cloudbow attenuation near 140° and the increase of polarized signal in the forward scattering direction as illustrated in Figure 6 (dashed lines). In the algorithm, the underneath cloud is assumed to be homogeneous. Nevertheless, the aerosol above cloud algorithm can be impacted but the sub-pixel cloud heterogeneity or fractional cloud cover, either because of a misclassification of aerosol layer above cloud case or with an erroneous retrieved AOT.

The misclassification of the scene could happen as 3D clouds effects increase the polarized reflectances in the forward scattering direction at 490 nm and consequently the Rayleigh pressures. To check the AOT value retrieved in this case, we use the polarized reflectances of the fractional cloud case. 3D polarized reflectances used as input of the algorithm and the ones simulated after the adjustment of the aerosol model and optical thickness are plotted in Figure 5 (solid lines).

For a scattering angular range between 60 and 180°, the algorithm works well. The lateral polarized reflectances in directions between 80° and 120° are quite low and consequently no aerosol (AOT=0) were retrieved. We note however that the cloudbow is not well reproduced. In the POLDER measurements, the range of sampled scattering angles vary with the geographical position. In some cases, it can be limited. We tested the algorithm for only available data in the backscattering directions ($\theta > 120°$) (dashed lines in Figure 5). The cloudbow signal is then better matched but the inversion method retrieves erroneous AOT values of 0.31 at 670 nm and 0.28 at 865 nm instead of zero for both.

A second test is made with simulated reflectances of a biomass-burning layer above the fractional cloud. For the simulation, the AOT of the aerosol layer is fixed to 0.28 and 0.15, the single scattering albedo to 0.93 and 0.91 at 670 and 865 nm respectively. In order to have no errors related to the aerosol model, we used one of the biomass burning aerosol model included in the fast algorithm. The simulated 3D angular polarized reflectances in function of the scattering angles are presented in Figure 6 (solid blue and red lines). Compared to the 1D reflectances with aerosols above cloud (dashed blue and red lines), the cloud heterogeneities effects amplify the increase of the forward signal and the decrease of the cloudbow signal. As with molecular scattering (section 4.1), aerosol scattering contributes to enhance the polarized reflectances in the shadow and cloud-free parts leading to higher averaged polarized reflectances in the forward direction. In the side scattering between 100° and 130° and in the cloudbow direction (near 140°), the polarized reflectances are additionally attenuated because of the plane-parallel biases. Note that for other solar zenith angles (not shown here), only the attenuation due to the plane parallel bias appears as the range of scattering angles in the forward direction is limited to 100 and 80° for SZA=20° and SZA=40° respectively.

The results obtained with the operational algorithm are presented in Table 3. The difference of AOT retrieval between 1D and 3D inputs depends on the solar zenith angle and ranges from negative values for SZA=20° to positive values for SZA=60°. In other words, the 1D assumption leads to underestimate AOT above cloud at SZA=20° and overestimate it at SZA=60°. The case SZA=40° is between the two and no impact on the AOT above cloud appears. Following the flowchart presented in (Waquet et al., 2013, Fig. 4), as AOT is more than 0.1, the best fitting model among all the available models is a fine model (a biomass model). Consequently, only forward scattering angles below 130° are used.

For SZA=60°, information used is between 60° to 130°. There is an increase of the forward scattering signal due to 3D effects, which is comparable to a case with more aerosols above the cloud. The retrieved AOT is thus higher with a relative error up to 65%. For SZA=20°, the scattering angle range is much more limited and is between 100° and 130°. Polarized reflectances for SZA=20° are not shown here but the figure is similar to the ones at 60°. For this particular angular range, 3D effects tend to decrease the polarized reflectances because of the plane-parallel biases, which corresponds to a lower AOT. Consequently, the AOT retrieved under the 1D assumption is underestimated with error between -35 and -40%.

The Angström exponent is related to the ratio of two optical thicknesses at the two wavelengths and corresponds in the retrieval to the best-selected model. For SZA=20°, differences are mainly due the plane-parallel bias, which is close for the two wavelengths. The ratio and consequently the Angstrom exponent are thus not affected by cloud heterogeneity effects.

For SZA=60°, the 3D effects consists in increasing the polarized signal because of additional scattering in the clear sky parts. This increase is higher at 865 nm than at 670 nm. This leads to an erroneous model and a smaller angstrom exponent.

Note that, in the operational algorithm, the algorithm is not applied for pixels too heterogeneous. Those are filtered using the standard deviation of the COT retrieved at 1 km by MODIS that should not exceed 5. For the fractional cloud of this study, the value computed from the input cloud optical thickness (different from the retrieved one) is 7 so above.

5. Conclusion

This study used simulations to understand and quantify effects of cloud heterogeneities on POLDER total and polarized reflectances. We investigate the consequences of heterogeneous cloud radiative effects on the retrieve values of optical depth, effective radius, effective variance, cloud pressure and optical properties (optical thickness and Angstrom coefficient) of above cloud aerosol, provided by operational and research algorithms of the POLDER radiometer. 3D cloud fields were generated with the 3DCLOUD model (Szczap et al., 2014; Alkassem et al., 2017) and the 1D and 3D radiative transfer simulations were done with the Monte Carlo 3DMCPOL model (Cornet et al., 2010). Three types of heterogeneous water cloud were studied: a flat, a bumpy and a fractional cloud.

The reflectances simulated at small spatial scale (50 m) and averaged at the POLDER spatial scale (7 km x 7 km) are used as realistic input of the different cloud operational and research algorithms. In the case of the optical thickness and high solar illumination (SZA=20°), we obtain, as it was already shown in numerous studies, lower optical thickness than the averaged ones because of the plane-parallel bias. For POLDER, it leads to retrieve optical thicknesses underestimated by 10 or 35% depending on the cloud type. For oblique solar incidence, the POLDER algorithm yields to higher optical thickness in the backscattering direction due to solar illumination effects and much lower optical thickness (up to -70% for the fractional cloud) in the forward scattering direction due to the shadowing effects. The errors on cloud albedo are weaker with maximal bias for albedo between -5% for high solar illumination and +8% for solar zenith angle of 60°.

We next analyzed, for the first time, the cloud heterogeneities effects on polarized reflectances. We showed a reduction of the cloudbow and side reflectances due to the plane-parallel bias and the shadowing effects. In the forward scattering direction, the effects are spectrally dependent. For the shortest wavelength (490 nm), the molecular scattering in the shadow areas increases the averaged polarized signal and lead to an increase of the polarized reflectances. At 865 nm, the weak positive polarized reflectances of the shadow areas reduced the negative polarization of the clouds. However, even if the polarized angular signature is modified, the retrieved effective radius and effective variance are not too much affected because cloud heterogeneities do not modify the positions of the cloudbow and surpernumerary bows. The Rayleigh cloud top pressure is, in contrast, biased for a solar zenith angle of 60° by about 120 hPa corresponding to a cloud 1 km lower in the atmosphere.

We also tested the aerosol above cloud algorithm (Waquet et al., 2013). Even in the absence of aerosol, the algorithm retrieves non-negligible AOT value when only a limited range of scattering angles is available. With aerosols above a

fractional cloud, the AOT can be underestimated for a high solar elevation (SZA=20°) because of the plane-parallel bias and on contrary overestimated for low solar elevation (SZA=60°) because of the shadowed effects that increase polarized reflectances. The Angström exponent is affected by these "shadowing effects" for SZA=60° but not by the plane-parallel bias since the plan-parallel biases for 490 nm and 865 nm is almost spectrally neutral and since the information of the ratio of two wavelengths is used.

Assessment of retrieval errors due to cloud heterogeneity is challenging for the next generation of retrieval algorithms. Indeed, in the future, it appears crucial to have not only values of retrieved parameters but also estimations of their uncertainties. Realistic simulations with known input parameters are very useful tools to assess accurately theses errors including their dependence on the available angular sampling. Such simulations can also obviously be used to test the next generation of operational algorithms.

The Multi-viewing, Multi-Channel, Multi-Polarization Imaging mission (3MI) that will fly on METOP-A SG as part of EUMETSAT Polar System after 2021, will have a spatial resolution of 4 x 4 km. The plane-parallel bias is thus expected to be lower than for the POLDER instrument. In addition, as 3MI will be on the same platform as the Visible Infrared Imager (VII), a multispectral radiometer with a resolution of 500 m, the correction of the plane parallel biases may be possible while the multi-angular capability of 3MI would help to detect the illumination and shadowing effects. Methods to mitigate the 3D effects can also be developed as proposed for example by (Davis et al., 2013) to retrieve the aerosol amount in a mixture of cloud and aerosols.

6. Acknowledgements

This work has been supported by the French Programme National de Télédétection Spatiale (PNTS, http://www.insu.cnrs.fr/pnts) grant N° PNTS-2014-02 and by the Centre National d'Etudes Spatiales (CNES).

References

Alexandrov, M.D., Cairns, B., Emde, C., Ackerman, A.S., van Diedenhoven, B., 2012. Accuracy assessments of cloud droplet size retrievals from polarized reflectance measurements by the research scanning polarimeter. Remote Sens. Environ. 125, 92–111. https://doi.org/10.1016/j.rse.2012.07.012

Alkassem, A., Szczap, F., Cornet, C., shcherbakov, V., Gour, Y., Jourdan, O., C-Labonnote, L., Mioche, G., 2017. Effects of cirrus heterogeneity on lidar CALIOP/CALIPSO data. J. Quant. Spectrosc. Radiat. Transf.

Breon, F.M., Doutriaux-Boucher, M., 2005. A comparison of cloud droplet radii measured from space. IEEE Trans. Geosci. Remote Sens. 43, 1796–1805. https://doi.org/10.1109/TGRS.2005.852838

Bréon, F.-M., Goloub, P., 1998. Cloud droplet effective radius from spaceborne polarization measurements. Geophys. Res. Lett. 25, 1879–1882. https://doi.org/10.1029/98GL01221

Buriez, J.-C., Doutriaux-Boucher, M., Parol, F., Loeb, N.G., 2001. Angular Variability of the Liquid Water Cloud Optical Thickness Retrieved from ADEOS–POLDER. J. Atmospheric Sci. 58, 3007–3018. https://doi.org/10.1175/1520-0469(2001)058<3007:AVOTLW>2.0.CO;2

Buriez, J.-C., Parol, F., Cornet, C., Doutriaux-Boucher, M., 2005. An improved derivation of the top-of-atmosphere albedo from POLDER/ADEOS-2: Narrowband albedos. J. Geophys. Res. Atmospheres 110, D05202. https://doi.org/10.1029/2004JD005243

Buriez, J.C., Vanbauce, C., Parol, F., Goloub, P., Herman, M., Bonnel, B., Fouquart, Y., Couvert, P., Seze, G., 1997a. Cloud detection and derivation of cloud properties from POLDER. Int. J. Remote Sens. 18, 2785–2813. https://doi.org/10.1080/014311697217332

Buriez, J.C., Vanbauce, C., Parol, F., Goloub, P., Herman, M., Bonnel, B., Fouquart, Y., Couvert, P., Seze, G., 1997b. Cloud detection and derivation of cloud properties from POLDER. Int. J. Remote Sens. 18, 2785–2813. https://doi.org/10.1080/014311697217332

Cahalan, R.F., 1994. Bounded cascade clouds: albedo and effective thickness. Nonlinear Process. Geophys. 1, 156–167.

Cornet, C., C-Labonnote, L., Szczap, F., 2010. Three-dimensional polarized Monte Carlo atmospheric radiative transfer model (3DMCPOL): 3D effects on polarized visible reflectances of a cirrus cloud. J. Quant. Spectrosc. Radiat. Transf. 111, 174–186. https://doi.org/10.1016/j.jqsrt.2009.06.013

Cornet, C., Szczap, F., C.-Labonnote, L., Fauchez, T., Parol, F., Thieuleux, F., Riedi, J., Dubuisson, P., Ferlay, N., 2013. Evaluation of cloud heterogeneity effects on total and polarized visible radiances as measured by POLDER/PARASOL and consequences for retrieved cloud properties, in: AIP Conference Proceedings. Presented at the RADIATION PROCESSES IN THE ATMOSPHERE AND OCEAN (IRS2012): Proceedings of the International Radiation Symposium (IRC/IAMAS), AIP Publishing, pp. 99–102. https://doi.org/10.1063/1.4804717

Davis, A.B., Garay, M.J., Xu, F., Qu, Z., Emde, C., 2013. 3D radiative transfer effects in multi-angle/multispectral radio-polarimetric signals from a mixture of clouds and aerosols viewed by a non-imaging sensor. Presented at the Polarization Science and Remote Sensing VI, International Society for Optics and Photonics, p. 887309. https://doi.org/10.1117/12.2023733

Davis, A.B., Marshak, A., 2010. Solar radiation transport in the cloudy atmosphere: a 3D perspective on observations and climate impacts. Rep. Prog. Phys. 73, 26801. https://doi.org/10.1088/0034-4885/73/2/026801

Deschamps, P.-Y., Breon, F.-M., Leroy, M., Podaire, A., Bricaud, A., Buriez, J.-C., Seze, G., 1994. The POLDER mission: instrument characteristics and scientific objectives. IEEE Trans. Geosci. Remote Sens. 32, 598–615. https://doi.org/10.1109/36.297978

Fauchez, T., Dubuisson, P., Cornet, C., Szczap, F., Garnier, A., Pelon, J., Meyer, K., 2015. Impacts of cloud heterogeneities on cirrus optical properties retrieved from space-based thermal infrared radiometry. Atmos Meas Tech 8, 633–647.

https://doi.org/10.5194/amt-8-633-2015

Goloub, P., Deuze, J.L., Herman, M., Fouquart, Y., 1994. Analysis of the POLDER polarization measurements performed over cloud covers. IEEE Trans. Geosci. Remote Sens. 32, 78–88. https://doi.org/10.1109/36.285191

Iwabuchi, H., Hayasaka, T., 2002. Effects of Cloud Horizontal Inhomogeneity on the Optical Thickness Retrieved from Moderate-Resolution Satellite Data. J. Atmospheric Sci. 59, 2227–2242. https://doi.org/10.1175/1520-0469(2002)059<2227:EOCHIO>2.0.CO;2

Kato, S., Hinkelman, L.M., Cheng, A., 2006. Estimate of satellite-derived cloud optical thickness and effective radius errors and their effect on computed domain-averaged irradiances. J. Geophys. Res. Atmospheres 111, D17201. https://doi.org/10.1029/2005JD006668

Loeb, N.G., Coakley, J.A., 1998. Inference of Marine Stratus Cloud Optical Depths from Satellite Measurements: Does 1D Theory Apply? J. Clim. 11, 215–233. https://doi.org/10.1175/1520-0442(1998)011<0215:IOMSCO>2.0.CO;2

Loeb, N.G., Davies, R., 1996. Observational evidence of plane parallel model biases: Apparent dependence of cloud optical depth on solar zenith angle. J. Geophys. Res. Atmospheres 101, 1621–1634. https://doi.org/10.1029/95JD03298

Loeb, N.G., Várnai, T., Winker, D.M., 1998. Influence of Subpixel-Scale Cloud-Top Structure on Reflectances from Overcast Stratiform Cloud Layers. J. Atmospheric Sci. 55, 2960–2973. https://doi.org/10.1175/1520-0469(1998)055<2960:IOSSCT>2.0.CO;2

Marbach, T., Riedi, J., Lacan, A., Schlüssel, P., 2015. The 3MI mission: multi-viewing-channel-polarisation imager of the EUMETSAT polar system: second generation (EPS-SG) dedicated to aerosol and cloud monitoring, Proc SPIE 9613, Polarization Science and Remote Sensing VII, 961310, https://doi.org/10.1117/12.2186978

Marshak, A., Davis, A. (Eds.), 2005. 3D Radiative Transfer in Cloudy Atmospheres, Physics of Earth and Space Environments. Springer-Verlag, Berlin/Heidelberg.

Marshak, A., Platnick, S., Várnai, T., Wen, G., Cahalan, R.F., 2006. Impact of three-dimensional radiative effects on satellite retrievals of cloud droplet sizes. J. Geophys. Res. Atmospheres 111, D09207. https://doi.org/10.1029/2005JD006686

Nakajima, T., King, M.D., 1990. Determination of the Optical Thickness and Effective Particle Radius of Clouds from Reflected Solar Radiation Measurements. Part I: Theory. J. Atmospheric Sci. 47, 1878–1893. https://doi.org/10.1175/1520-0469(1990)047<1878:DOTOTA>2.0.CO;2

Parol, F., Buriez, J.C., Vanbauce, C., Riedi, J., C.-Labonnote, L., Doutriaux-Boucher, M., Vesperini, M., Sèze, G., Couvert, P., Viollier, M., Bréon, F.M., 2004. Review of capabilities of multi-angle and polarization cloud measurements from POLDER. Adv. Space Res., Climate Change Processes in the Stratosphere, Earth-Atmosphere-Ocean Systems, and Oceanographic Processes from Satellite Data 33, 1080–1088. https://doi.org/10.1016/S0273-1177(03)00734-8

Platnick, S., King, M.D., Ackerman, S.A., Menzel, W.P., Baum, B.A., Riedi, J.C., Frey, R.A., 2003. The MODIS cloud products: algorithms and examples from Terra. IEEE Trans. Geosci. Remote Sens. 41, 459–473. https://doi.org/10.1109/TGRS.2002.808301

Szczap, F., Gour, Y., Fauchez, T., Cornet, C., Faure, T., Jourdan, O., Penide, G., Dubuisson, P., 2014. A flexible three-

dimensional stratocumulus, cumulus and cirrus cloud generator (3DCLOUD) based on drastically simplified atmospheric equations and the Fourier transform framework. Geosci Model Dev 7, 1779–1801. https://doi.org/10.5194/gmd-7-1779-2014

Szczap, F., Isaka, H., Saute, M., Guillemet, B., Ioltukhovski, A., 2000a. Effective radiative properties of bounded cascade nonabsorbing clouds: Definition of the equivalent homogeneous cloud approximation. J. Geophys. Res. Atmospheres 105, 20617–20633. https://doi.org/10.1029/2000JD900146

Szczap, F., Isaka, H., Saute, M., Guillemet, B., Ioltukhovski, A., 2000b. Effective radiative properties of bounded cascade absorbing clouds: Definition of an effective single-scattering albedo. J. Geophys. Res. Atmospheres 105, 20635–20648. https://doi.org/10.1029/2000JD900145

Varnai, T., 2000. Influence of Three-Dimensional Radiative Effects on the Spatial Distribution of Shortwave Cloud Reflection. J. Atmospheric Sci. 57, 216–229. https://doi.org/10.1175/1520-0469(2000)057<0216:IOTDRE>2.0.CO;2

Varnai, T., Davies, R., 1999. Effects of Cloud Heterogeneities on Shortwave Radiation: Comparison of Cloud-Top Variability and Internal Heterogeneity. J. Atmospheric Sci. 56, 4206–4224. https://doi.org/10.1175/1520-0469(1999)056<4206:EOCHOS>2.0.CO;2

Varnai, T., Marshak, A., 2002. Observations of Three-Dimensional Radiative Effects that Influence MODIS Cloud Optical Thickness Retrievals. J. Atmospheric Sci. 59, 1607–1618. https://doi.org/10.1175/1520-0469(2002)059<1607:OOTDRE>2.0.CO;2

Waquet, F., Cornet, C., Deuzé, J.-L., Dubovik, O., Ducos, F., Goloub, P., Herman, M., Lapyonok, T., Labonnote, L.C., Riedi, J., Tanré, D., Thieuleux, F., Vanbauce, C., 2013. Retrieval of aerosol microphysical and optical properties above liquid clouds from POLDER/PARASOL polarization measurements. Atmos Meas Tech 6, 991–1016. https://doi.org/10.5194/amt-6-991-2013

Waquet, F., Riedi, J., Labonnote, L.C., Goloub, P., Cairns, B., Deuzé, J.-L., Tanré, D., 2009. Aerosol Remote Sensing over Clouds Using A-Train Observations. J. Atmospheric Sci. 66, 2468–2480. https://doi.org/10.1175/2009JAS3026.1

Zeng, S., Cornet, C., Parol, F., Riedi, J., Thieuleux, F., 2012. A better understanding of cloud optical thickness derived from the passive sensors MODIS/AQUA and POLDER/PARASOL in the A-Train constellation. Atmos Chem Phys 12, 11245–11259. https://doi.org/10.5194/acp-12-11245-2012

Zeng, S., Parol, F., Riedi, J., Cornet, C., Thieuleux, F., 2011. Examination of POLDER/PARASOL and MODIS/Aqua Cloud Fractions and Properties Representativeness. J. Clim. 24, 4435–4450. https://doi.org/10.1175/2011JCLI3857.1

Zeng, S., Riedi, J., Parol, F., Cornet, C., Thieuleux, F., 2013. An assessment of cloud top thermodynamic phase products obtained from A-Train passive and active sensors. Atmos Meas Tech Discuss 6, 8371–8411. https://doi.org/10.5194/amtd-6-8371-2013

Zhang, Z., Ackerman, A.S., Feingold, G., Platnick, S., Pincus, R., Xue, H., 2012. Effects of cloud horizontal inhomogeneity and drizzle on remote sensing of cloud droplet effective radius: Case studies based on large-eddy simulations. J. Geophys. Res. Atmospheres 117, D19208. https://doi.org/10.1029/2012JD017655

Zhang, Z., Werner, F., Cho, H.-M., Wind, G., Platnick, S., Ackerman, A.S., Di Girolamo, L., Marshak, A., Meyer, K., 2016.

A framework based on 2-D Taylor expansion for quantifying the impacts of subpixel reflectance variance and covariance on cloud optical thickness and effective radius retrievals based on the bispectral method. J. Geophys. Res. Atmospheres 121, 2016JD024837. https://doi.org/10.1002/2016JD024837

Zhou, Y., Sun, X., Zhang, R., Zhang, C., Li, H., Zhou, J., Li, S., 2017. Influences of cloud heterogeneity on cirrus optical properties retrieved from the visible and near-infrared channels of MODIS/SEVIRI for flat and optically thick cirrus clouds. J. Quant. Spectrosc. Radiat. Transf. 187, 232–246. https://doi.org/10.1016/j.jqsrt.2016.09.020

Zinner, T., Mayer, B., 2006. Remote sensing of stratocumulus clouds: Uncertainties and biases due to inhomogeneity. J. Geophys. Res. Atmospheres 111, D14209. https://doi.org/10.1029/2005JD006955

Atmos. Meas. Tech. Discuss., https://doi.org/10.5194/amt-2017-413
Manuscript under review for journal Atmos. Meas. Tech.
Discussion started: 4 December 2017

Atmospheric Measurement Techniques Discussions

Cloud Albedo	Sun incidence	SZA=20°	SZA=40°	SZA=60°
Homo Cloud (1D)	Simulation	0.434	0.498	0.601
	Retrieval	0.434	0.496	0.600
	Error (%)	**-0.04**	**-0.46**	**-0.16**
Flat Cloud	Simulation	0.390	0.458	0.556
	Retrieval	0.382	0.445	0.569
	Error (%)	**-2.09**	**-2.80**	**+2.35**
Bumpy Cloud	Simulation	0390	0.451	0.562
	Retrieval	0.380	0.450	0.583
	Error (%)	**-2.44**	**-0.26**	**+3.69**
Fractional Cloud	Simulation	0.301	0.353	0.475
	Retrieval	0.287	0.353	0.513
	Error (%)	**-4.71**	**+0.14**	**+7.88**

Table 1: For each cloud, cloud albedo simulation with 3DMCPOL (first line), retrieved with the POLDER operational algorithm (second line) and relative differences [(Retrieval-Simulation)/Simulation x 100] between the two values (third line) for the homogeneous cloud (for control), for the flat, bumpy and fractional clouds for three solar zenith angles (20, 40 and 60°). The mean optical thickness of each cloud is 10 and the effective radius

Atmos. Meas. Tech. Discuss., https://doi.org/10.5194/amt-2017-413
Manuscript under review for journal Atmos. Meas. Tech.
Discussion started: 4 December 2017

Atmospheric Measurement Techniques Discussions

	Input	Homogeneous cloud (1D)	Flat cloud	Bumpy cloud	Fractional cloud
Reff (µm)	11.00	11.04	11.12	11.08	11.33
Veff	0.02	0.019	0.021	0.019	0.023
CTOP (hPa) /(km)	868/1.23	860/1.31	903/0.92		
	833/1.56	854/1.36		925/0.73	
	803/1.86	823/1.66			946/0.55
Cost function		8.45	30.07	63.43 (NC)	351.4 (NC)

Table 2: Retrieved effective radius (Reff), effective variance (Veff) and cloud top altitude (CTOP) from polarized reflectances with an optimal estimation algorithm. First column is the input, second column the retrieval for the homogeneous cloud (1D), third column for the flat cloud, fourth column for the bumpy cloud and fifth column for the fractional cloud. Last line is the final cost function with NC meaning no convergence. The solar zenith angle is 60°. Note that the cloud top altitude is different according to the heterogeneous cloud leading to three different lines.

Atmos. Meas. Tech. Discuss., https://doi.org/10.5194/amt-2017-413
Manuscript under review for journal Atmos. Meas. Tech.
Discussion started: 4 December 2017

Atmospheric Measurement Techniques Discussions

	Sun incidence	SZA=20°	SZA=40°	SZA=60°
AOT670	Homogeneous cloud	0.337	0.319	0.319
	Fractional cloud	0.225	0.319	0.491
	Difference (%)	**-33.2**	**0.00**	**+53.9**
AOT865	Homogeneous cloud	0.180	0.170	0.170
	Fractional cloud	0.119	0.170	0.280
	Difference (%)	**-33.9**	**0.00**	**+64.7**
Angstrom coefficient	Homogeneous cloud	2.46	2.46	2.46
	Fractional cloud	2.46	2.46	2.20
	Difference (%)	**0.00**	**0.00**	**-10.6**

Table 3: Retrieved aerosol properties for a biomass aerosol layer above the fractional cloud with the operational algorithm described in (Waquet et al., 2013) : aerosol optical thickness at 670 nm (AOT670), at 865 nm (AOT865) and Angström coefficient for three solar zenith angles (SZA).

Atmos. Meas. Tech. Discuss., https://doi.org/10.5194/amt-2017-413
Manuscript under review for journal Atmos. Meas. Tech.
Discussion started: 4 December 2017

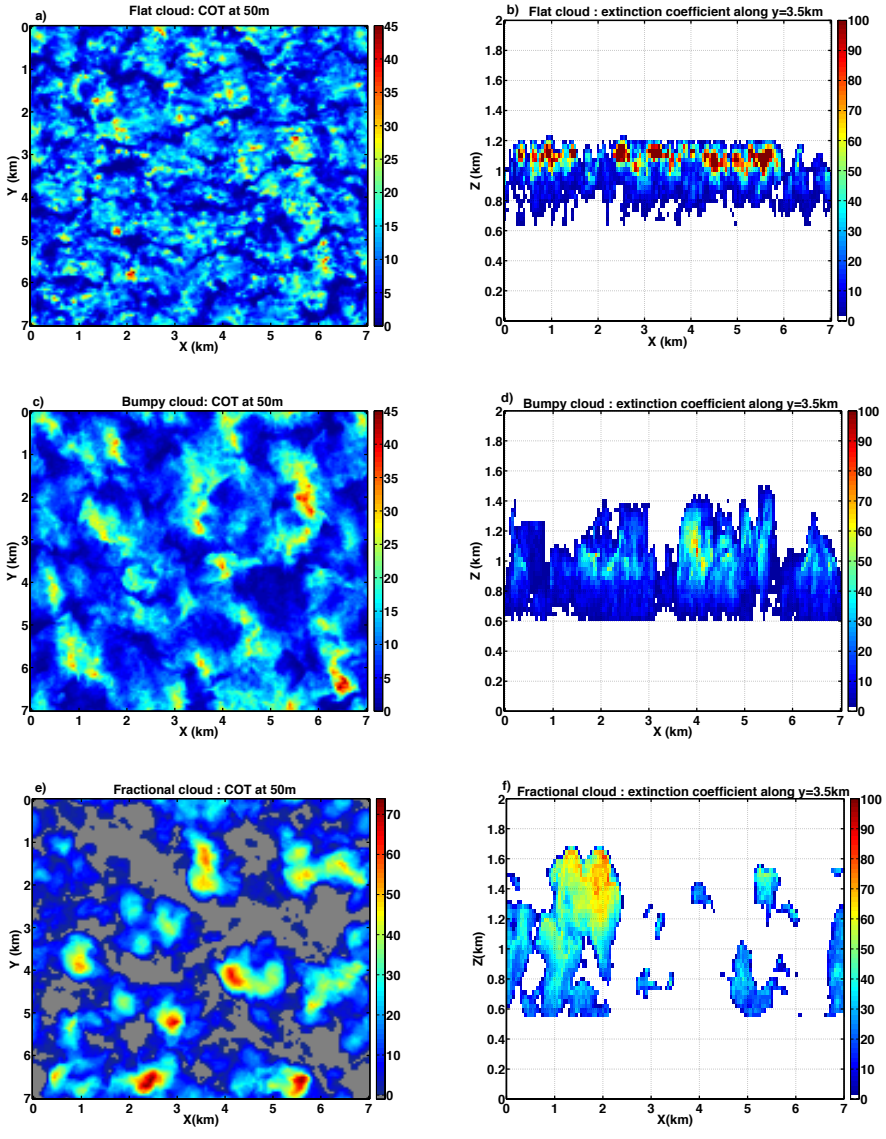

Figure 1: Cloud optical thickness (COT) of the three clouds used for the study (a) the flat cloud, (c) the bumpy cloud and (e) the fractional cloud. Extinction coefficient (km^{-1}) along the x-z axis for y=3.5 km for the flat cloud (b) the bumpy cloud (d) and the fractional cloud (f).

Atmos. Meas. Tech. Discuss., https://doi.org/10.5194/amt-2017-413
Manuscript under review for journal Atmos. Meas. Tech.
Discussion started: 4 December 2017

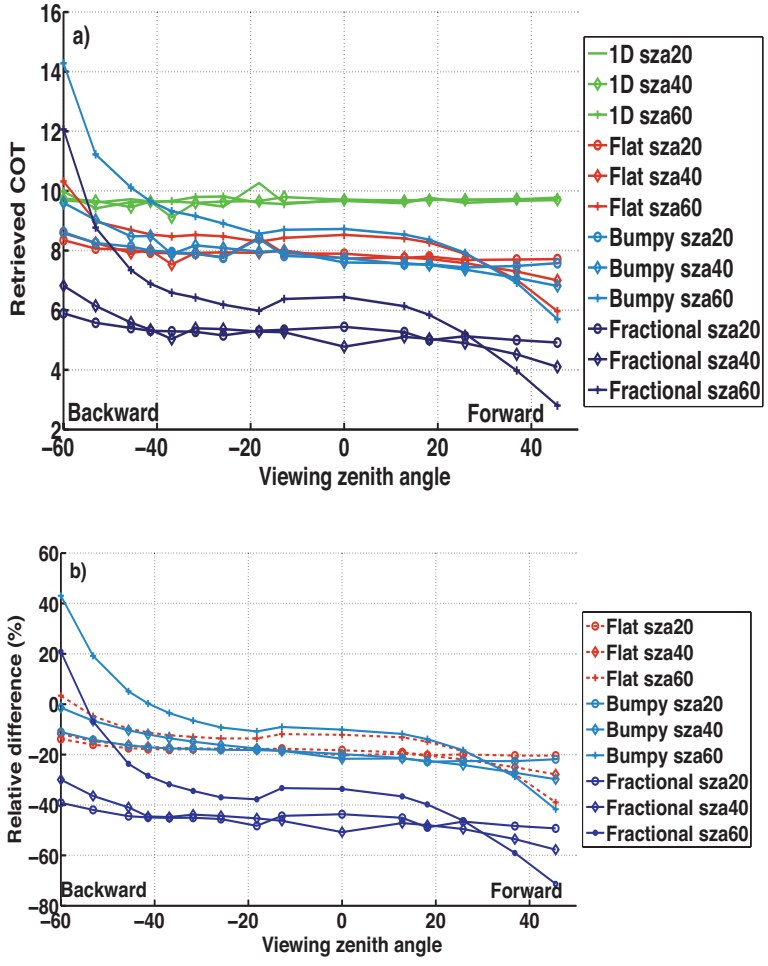

Figure 2 (a): Cloud optical thickness (COT) retrieved with the POLDER operational algorithm as function of the viewing zenith angle for the four different simulated cloud cases (1D, flat, bumpy and fractional clouds) and for different solar zenith angles (20, 40 and 60°). (b) Relative differences [(COT3D-COT1D)/COT1D x 100] between the heterogeneous cloud (3D) and the homogenous cloud (1D) COT

Atmos. Meas. Tech. Discuss., https://doi.org/10.5194/amt-2017-413
Manuscript under review for journal Atmos. Meas. Tech.
Discussion started: 4 December 2017

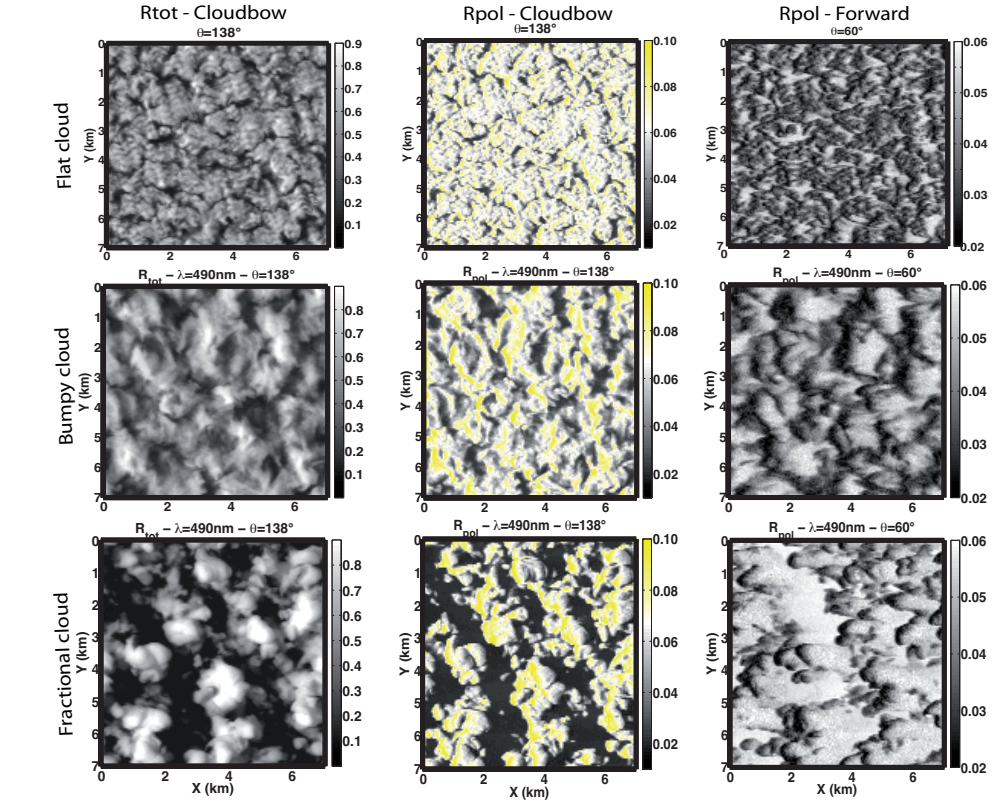

Figure 3: Total and polarized reflectances for the flat cloud (first line), the bumpy cloud (second line) and the fractional cloud (third line). Total reflectances at 490 nm in the forward scattering direction (first column), polarized reflectances at 490 nm in the cloudbow direction (second column) and polarized reflectances at 490 nm in the forward direction (third column). The Sun illuminates the scene from the left of the figures (SZA=60°). For polarized reflectances in the second column, yellow color corresponds to values higher than the maximum value predicted by the homogeneous cloud assumption.

Atmos. Meas. Tech. Discuss., https://doi.org/10.5194/amt-2017-413
Manuscript under review for journal Atmos. Meas. Tech.
Discussion started: 4 December 2017

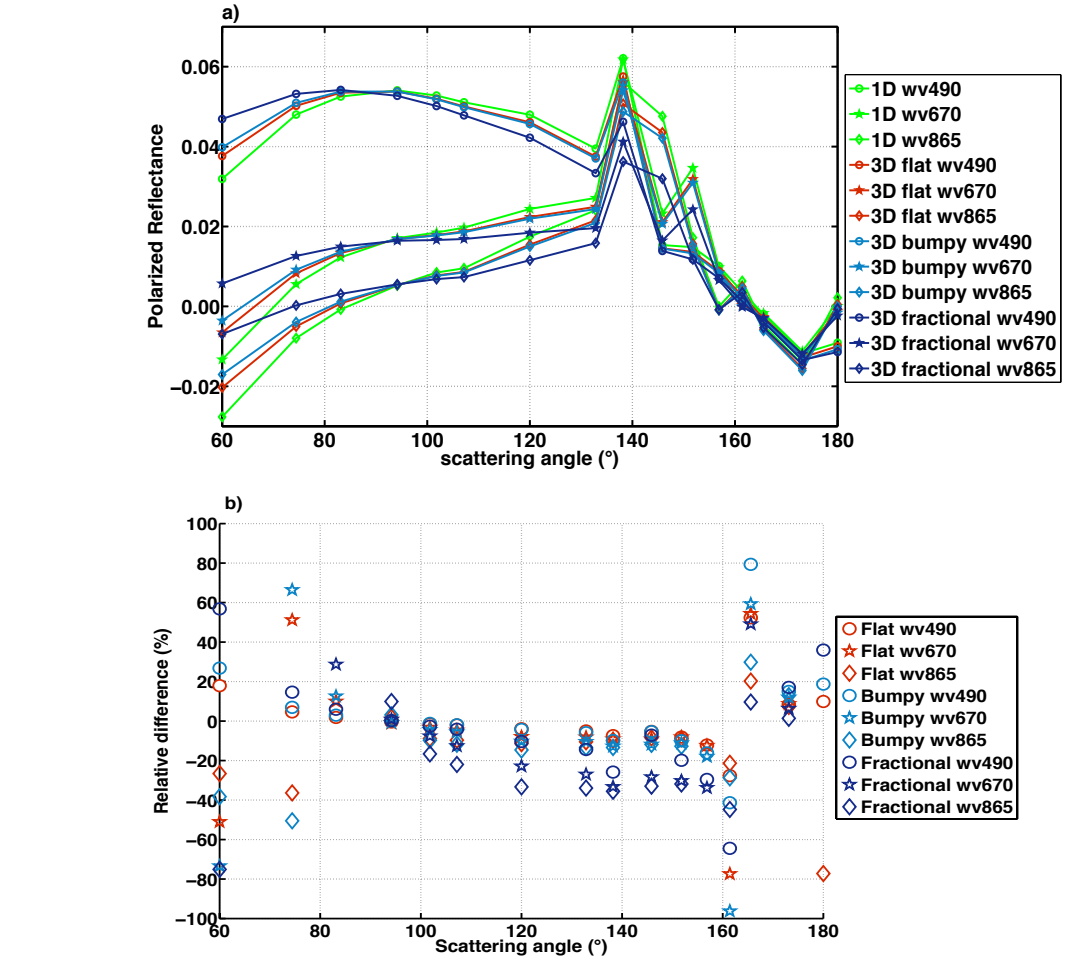

Figure 4: Polarized reflectances (SZA=60°) as function of the scattering angle for three wavelengths (490 nm, 670 nm, 865 nm) for the homogeneous cloud (1D), the flat cloud, the bumpy cloud and the fractional cloud (a). Relative difference between 3D and 1D polarized reflectances, (Rp3D-Rp1D)/Rp1D*100 (b). The solar incidence is 60°.

Atmos. Meas. Tech. Discuss., https://doi.org/10.5194/amt-2017-413
Manuscript under review for journal Atmos. Meas. Tech.
Discussion started: 4 December 2017

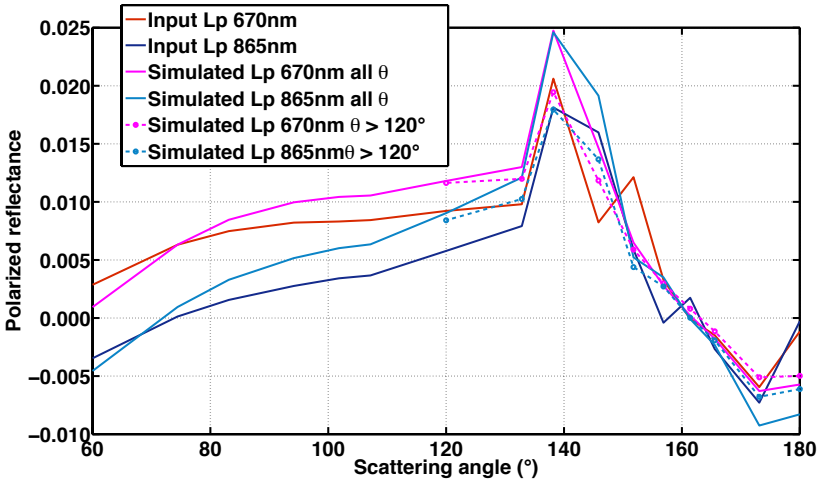

Figure 5: 3D Polarized reflectances used as input for the Aerosol Above Cloud algorithm (Waquet et al., 2013) and polarized reflectances simulated with the algorithm after the convergence of the retrieval. Reflectances at all angles were used (solid line) and reflectances with only scattering angles above 120° (dotted line).

Atmos. Meas. Tech. Discuss., https://doi.org/10.5194/amt-2017-413
Manuscript under review for journal Atmos. Meas. Tech.
Discussion started: 4 December 2017

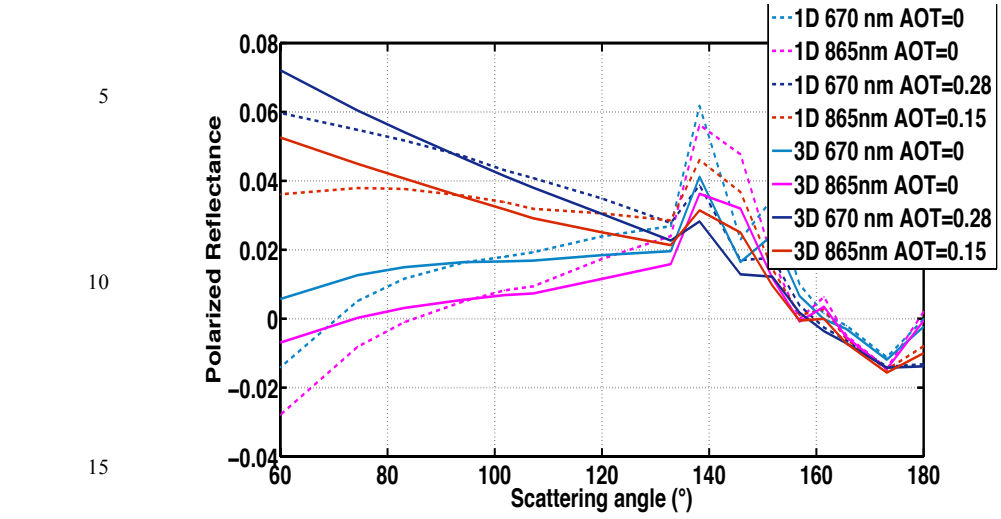

Figure 6: Polarized reflectances as function of the scattering angle. Dashed lines are for homogeneous cloud without and with a biomass burning aerosol layer above; solid lines are for the fractional cloud without and with a biomass burning aerosol layer above. The solar incidence angle is 60°.